IEEE Journal of Microwaves

Received 26 September 2024; revised 16 November 2024; accepted 12 December 2024.

Digital Object Identifier 10.1109/JMW.2024.3518555

Millimeter-Wave Retrodirective Wireless Power Transfer Applicable to Small Electronic Devices

SOOYOUNG OH [1] (Graduate Student Member, IEEE), DO HYEON KIM [2] (Graduate Student Member, IEEE), WONWOO LEE [3], JUNHYUK YANG [1], CHANGKUN PARK [1,2,3] (Member, IEEE), HOJIN LEE [1,2,3] (Member, IEEE), AND SUN K. HONG [1,2,3] (Senior Member, IEEE)

(Regular Paper)

[1]Department of Electronic Engineering, Soongsil University, Seoul 06978, South Korea
[2]Department of Intelligent Semiconductors, Soongsil University, Seoul 06978, South Korea
[3]Department of Information Communication Convergence Technology, Soongsil University, Seoul 16978, South Korea

CORRESPONDING AUTHOR: Sun K. Hong (e-mail: shong215@ssu.ac.kr).

This work was supported in part by the Office of Naval Research under Grant N00014-23-1-2648; and in part by the National Research Foundation of Korea funded by the Korea Government (MSIT) under Grant RS-2023-00218972.

ABSTRACT With the recent surge in popularity of the Internet of Things (IoT), there also has been a notable increase in research on wirelessly charging IoT enabled electronic devices. Millimeter-wave retrodirective power beaming has recently emerged as a suitable candidate for wirelessly charging small electronic devices. In this paper, we propose and demonstrate a millimeter-wave power beaming concept applicable to IoT ecosystem. The proposed system incorporates a Rotman lens retrodirective beamformer as a Tx unit. To demonstrate the retrodirective power beaming, a Rotman lens beamformer on a waveguide platform is designed to operate at Ka-band. The proposed Rotman lens operates with seven beam ports capable of radiating seven beams within $\pm 30°$ steering range. On the receiving end, a rectenna consisting of a patch array and rectifier is designed. We then conducted an end-to-end power beaming experiment as proof of concept, where the results demonstrate the capability of the proposed system as a retrodirective millimeter-wave power beaming system.

INDEX TERMS Internet of things (IoT), millimeter-wave (mmWave), retrodirective, power beaming, Rotman lens.

I. INTRODUCTION

The Internet of Things (IoT) has become increasingly popular in the last decade due to its grand objective of interconnecting almost everything [1]. It is anticipated that in the near future, a vast number of IoT devices will be utilized to reach their goal. Along with a cellular phone which is a typical example of an IoT device, small autonomous aerial vehicles (AAVs), also known as drones, are widely becoming a part of the IoT ecosystem as they expand their usability for gathering and transmitting data, such as monitoring and surveillance purposes [2]. Moreover, the usage of smart sensors and wearable smartwatches is steadily on the rise as they are gaining popularity. However, as with every wireless device, battery-powered drones and sensors have a limited usable time and must be recharged at some point. Requirement of charging is a common challenge faced by not only the aforementioned devices, but also every IoT-enabled electronic device. This consequently leads to a growing demand for wirelessly charging through wireless power transfer (WPT) [3], [4], [5], [6], [7].

To address this demand for wireless charging, power beaming concept can be utilized, which can be thought of as a subset of WPT. In contrast to near-field WPT, i.e., inductive coupling, whose range is generally limited to few tens of centimeters, power beaming operates either in the Fresnel or far-field region, enabling power transfer at much longer distances [8]. A way to enhance the transmission efficiency is to increase the aperture size of the beamformer. However, most of

the recent power beaming technologies have been researched in the microwave regime (below 10 GHz) [9], [10], [11], [12]. With the development of mobile communications and IoT technology, devices are being miniaturized. As the form factor decreases, the size of the antenna embedded in these devices should also decrease. Therefore, it is necessary to generate narrow beams to direct power at the devices of interest.

Millimeter-waves (mmWaves) which is commonly referred to the frequencies above 24 GHz, mitigate the size issues associated with microwave frequencies. Since mmWaves have wavelengths significantly shorter than that of microwave, they demonstrate higher directivity given the smaller aperture size, thereby achieving narrower beams. Moreover, high directivity makes it convenient for beam controlling/beam focusing while minimizing the focusing area. Therefore, power beaming with mmWaves has gained increased attention in remote charging of small devices in meter-range applications and expected to be a promising technology for wirelessly charging compact electronic devices [13], [14], [15], [16], [17].

As stated above, when employing mmWaves power beaming, it is essential to precisely direct the beam at the receiver to efficiently deliver energy. Therefore, a retrodirective operation is beneficial [18], [19], [20], [21], [22]. That is, the transmit array should be able to direct the beam at a device of interest upon the receipt of a beacon or pilot signal sent from the device. The core concept of retrodirectivity lies in reversing the time-delay or phase profile of the waves received by the array elements. Fig. 1 illustrates a notional scheme of an end-to-end retrodirective power beaming system applied to IoT ecosystem. The beacon signals are transmitted from various kinds of IoT devices, e.g., sensors, mobile devices, and drones. The beamformer equipped with an array antenna then receives the beacon signal implying the device is in a low battery status. The beacon signal passes through the T/R modules, which in this case arrives at the Rx unit. Once the relative time/phase delay of the received antenna at each element of the array is calculated, the Tx unit allows to re-transmit the power to the corresponding direction allowing for wireless charging of the device in need.

Among various methods for constructing retrodirective beamforming network, Rotman lens provides a simple solution for achieving retrodirectivity [21], [23], [24], [25], [26], [27], [28], [29], [30], [31], [32]. The true-time-delay (TTD) within the lens facilitates self-phasing, resulting in the redirection of the beam towards the intended target. The Rotman lens, implementing TTD without the necessity for phase shifters to reverse phase (time), inherently supports wide bandwidth and achieves all-passive control for beamforming. This eliminates the requirement for a complex feed network for active beamforming. The design of mmWaves beamformer based on Rotman lens have been reported on various platforms such as microstrip [21], [28], [29] and substrate integrated waveguides (SIWs) [30], [31], [32]. To enhance the power beaming range, it is essential to design the Rotman lens on a platform with low losses and superior power handling capabilities to achieve higher-power and higher-gain operation.

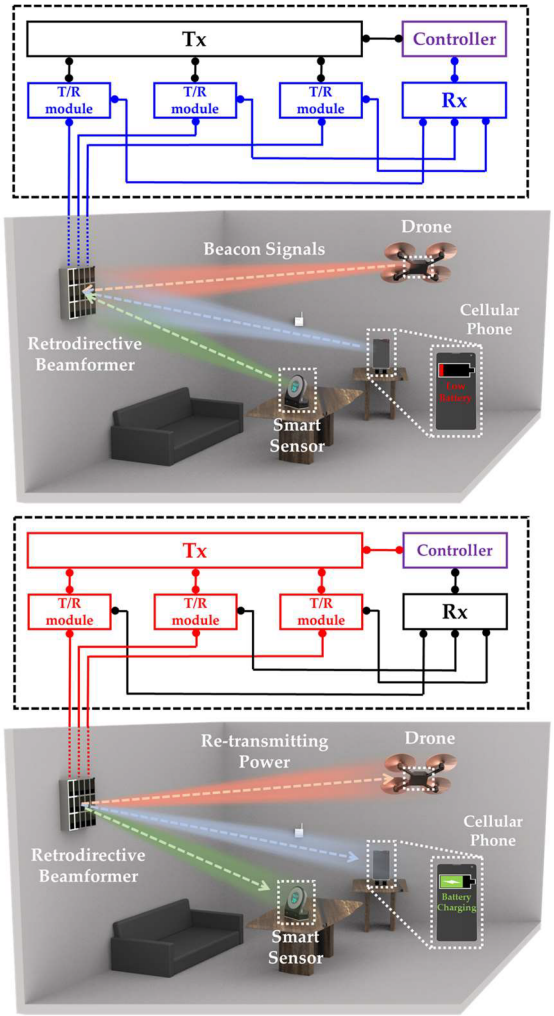

FIGURE 1. Conceptual illustration of the proposed retrodirective power beaming.

For this purpose, this paper introduces a notional end-to-end mmWaves power beaming concept based on a Rotman lens beamformer as a Tx unit and rectennas as Rx unit. The proposed Rotman lens is designed on a waveguide platform to exhibit lower loss and enhanced power handling, while it operates at Ka-band with a center frequency of 33 GHz. The Rotman lens is designed to have seven input beam ports and eight array ports, which makes it capable of radiating seven beams within $\pm 30^{\circ}$ of steering range. Moreover, rectenna is designed to target the same center frequency. Ultimately, we experimentally demonstrate the power beaming using the aforementioned devices as proof of concept. The organization of the paper is as follows. The design methodology of the proposed Rotman lens and simulated/measured results are dealt in Section II. Section III presents the design and results of the rectenna, while the power beaming experiment with the Rotman lens and rectenna is presented in Section IV, while the results and the expandability of the system are discussed in Section V. Section VI concludes the paper with a summary and implications of the results.

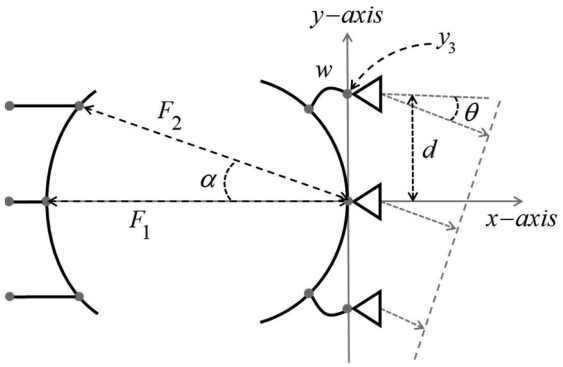

FIGURE 2. Configuration of rotman lens with design parameters.

II. WAVEGUIDE ROTMAN LENS AS TRANSMITTER

A. ROTMAN LENS DESIGN METHODOLOGY

There are several design requirements that need to be specified when designing a Rotman lens as depicted in Fig. 2 [23]. The designer should determine the center frequency (f_0). Then, the number of beam ports (M) and number of array ports (N) is fined by half-power beamwidth (HPBW) of array and maximum scan angle (θ_0) as follows:

$$M = \frac{2\theta_0}{beamwidth} \tag{1}$$

After determining the design requirements, the beam and array contours that construct the lens are based on the parameters, F_1,α, β, ξ. The geometrical condition of an on-axis focal length F_1 is defined as:

$$F_1 \geq 2\,(N-1)\,d\,\sin\theta_0. \tag{2}$$

α is the angle between two focal lengths, β is the ratio of on-axis and off-axis focal lengths as:

$$\beta = F_2 / F_1, \tag{3}$$

while indirect parameter ξ controls the amplitude and phase error of the lens:

$$\xi = y_3 \gamma / F_1. \tag{4}$$

Here, y_3 is the y-axis position where antenna element array is placed, and γ is the expansion factor which is the ratio between the focal angle α and array beam angle θ:

$$\gamma = \sin\theta / \sin\alpha. \tag{5}$$

The geometric lens equation can be expressed as a quadratic equation in the line length w, representing the connection between an array port and its corresponding antenna element:

$$a\left(w/F_1\right)^2 + b\left(w/F_1\right) + c = 0, \tag{6}$$

where the coefficients a, b, and c can be expressed as follows [23], [24], [25]:

$$a = 1 - \frac{(1-\beta)^2}{(1-\beta\cos\alpha)^2} - \frac{\xi^2}{\beta^2}, \tag{7}$$

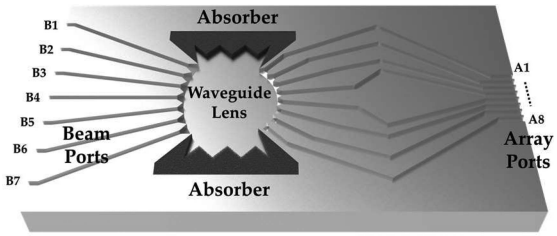

FIGURE 3. Cross-sectional view of the proposed rotman lens.

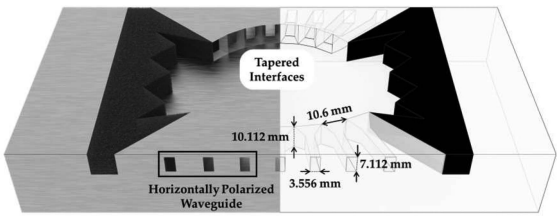

FIGURE 4. Detailed view of the tapered interface of waveguide-to-lens.

$$b = -2 + \frac{2\xi^2}{\beta} + \frac{2\,(1-\beta)}{1-\beta\cos\alpha} - \frac{\xi^2\sin^2\alpha\cdot(1-\beta)}{(1-\beta\cos\alpha)^2}, \tag{8}$$

$$c = -\xi^2 + \frac{\xi^2\sin^2\alpha}{1-\beta\cos\alpha} - \frac{\xi^4\sin^4\alpha}{4(1-\beta\cos\alpha)^2}. \tag{9}$$

B. DESIGN OF THE ROTMAN LENS ON WAVEGUIDE PLATFORM

The designed waveguide Rotman lens comprises seven input beam ports and eight output array ports, which makes it capable of generating seven beams within ±30° of steering range with a 10° increment. Under the design formulas mentioned in the previous subsection, the position of the beam and array ports are arranged. The relative length (w/F_1) of the transmission line between array ports and the antenna array is also calculated. Fig. 3 illustrates the cross-sectional view of the Rotman lens designed on a waveguide platform.

When designing waveguide-based Rotman lens, it is common for waveguide to facilitate vertical polarization (width and length of 3.556 mm and 7.112 mm) to mitigate diffraction level. However, in order to realize the array interval of 0.5 λ, the waveguide utilized here is rotated by 90°, facilitating horizontal polarization (width and length of 7.112 mm and 3.556 mm). Upon achieving the horizontal polarization, each junction between port and lens is tapered to have a cross-section of 10.6 mm × 10.112 mm to mitigate the diffraction, which can be seen in Fig. 4. Since there is a height difference between the waveguide and the lens, the actual phase difference (path length difference) of wave differs from that obtained by the design formula. Therefore, compensation needs to be made accordingly by conducting a numerical simulation to align the phase difference. Fig. 5 compares the phase profile at the array elements resulting from feeding at different beam ports: calculated (dashed) and simulated (solid). The calculated phase

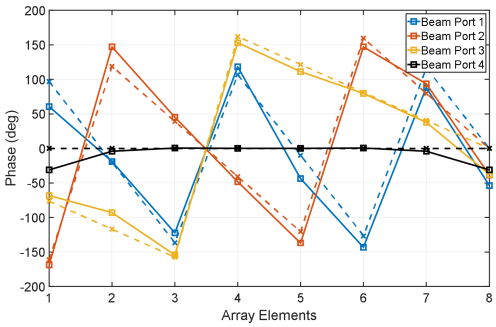

FIGURE 5. **Phase profile at the array elements resulting from feeding at different beam ports: calculated (dashed) and simulated (solid).**

is derived from the simple array equation as [33]:

$$l_{path} = (N-1) \cdot d \cdot \cos\left(90^\circ - \theta\right), \tag{10}$$

where l_{path} represents the relative wave travel distance required to generate the beam at θ with A1 (see Fig. 3) as the reference point. Since the proposed Rotman lens is designed to have $\pm 30^\circ$ of steering range with a 10° increment, θ should be set accordingly to the steering angle. The calculated and simulated phase shows a close agreement with a slight discrepancy, which can be explained by observing port 4 (black lines). However, this discrepancy is not crucial to beam pointing ability where it will be shown in the next subsection.

The antenna array ports of the waveguide beamformer are then connected to an array of eight horn antennas to provide high gain. Since the waveguide is positioned to have horizontal polarization, the horn antenna is designed to be an H-plane sectoral horn antenna while maintaining the array spacing and the width of each cross-section of the waveguide at the array ports. The overall cross-sectional view of the total structure is illustrated in Fig. 6(a) and the fabricated structure is shown in Fig. 6(b) with a total volume of 438.2 mm $\times$ 160 mm $\times$ 85 mm.

C. SIMULATED AND MEASURED RESULTS OF ROTMAN LENS BEAMFORMER

The proposed waveguide Rotman lens is validated via full-wave simulation using CST Studio Suite. Fig. 7(a) includes the simulated reflection coefficients at the first four beam ports (since ports 5–7 are symmetric to ports 1–3), while Fig. 7(b) shows the measured reflection coefficients at all seven beam ports with an Anritsu MS46122B vector network analyzer. The simulated and measured reflection coefficients are both observed to be under -10 dB at all input beam ports, indicating good impedance matching over the entire Ka-band.

The radiation characteristics of the fabricated lens are measured in an anechoic chamber as shown in Fig. 8. By feeding each beam port of the Rotman lens at a time, the radiation characteristics and beamforming capabilities can be obtained. The simulated and measured radiation patterns of the waveguide Rotman lens at 32–34 GHz with an interval of 0.5 GHz are presented in Fig. 9. It can be observed that at the target

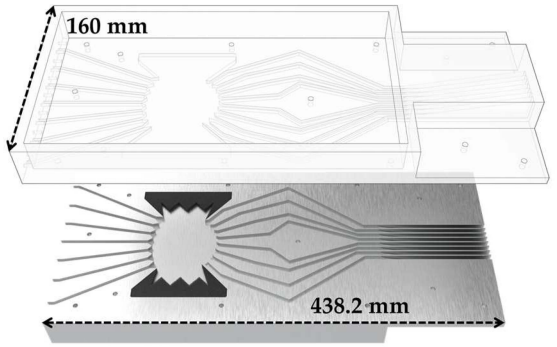

(a)

(b)

FIGURE 6. **(a) Cross-sectional view of the total structure, (b) fabricated Rotman lens.**

frequency of 33 GHz, the simulated (dashed line) and the measured (solid line) radiation patterns are in a good agreement with a gain difference of only 0.5 dB and a beam pointing error of 1°. The radiation patterns at other frequencies also exhibit the similarity between the simulated and measured values since the main beam radiates properly in a desired direction with a similar gain.

III. RECTENNA AS RECEIVER

In the previous section, the design methodology and performance of the waveguide Rotman lens are presented. The purpose of this section is to present the design of an appropriate receive-end that can properly receive RF power radiated from the transmitter, in order to experimentally demonstrate the end-to-end wireless power beaming. Here, we utilize a rectenna to convert RF power into DC power. As shown in Fig. 10, the rectenna consists of a 4×6 microstrip patch array followed by a rectifier. The designed rectenna is initially verified by separately testing the patch array and rectifier, which are later combined into a single structure for fabrication and experiment.

A. MICROSTRIP PATCH ARRAY DESIGN AND MEASUREMENT

Fig. 11 shows the microstrip patch array designed to operate at 33 GHz. The antenna array is printed on a Rogers 5880 ($\varepsilon_r = 2.2$) laminate with a thickness of 0.254 mm. The length and width of the patch elements are optimized to resonate

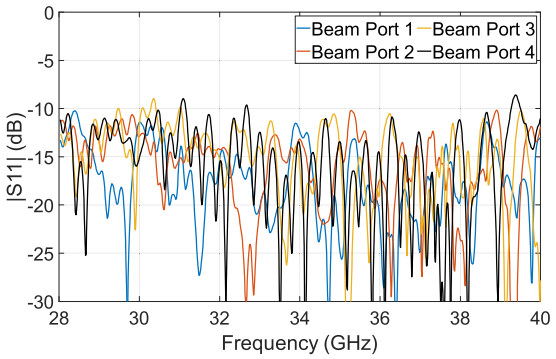

(a)

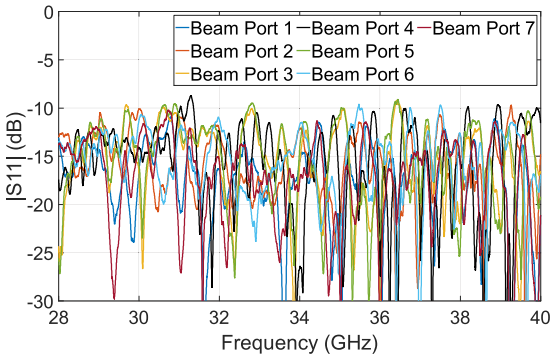

(b)

FIGURE 7. (a) Simulated reflection coefficients from port 1–4 (b) measured reflection coefficients from port 1–7.

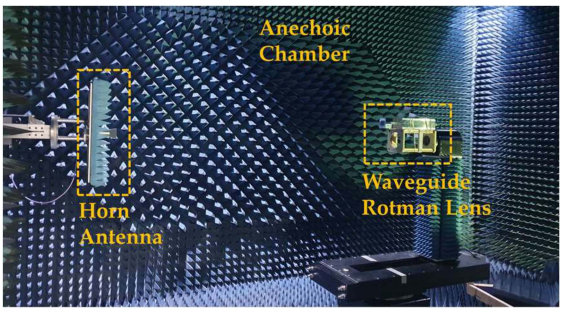

FIGURE 8. Radiation measurement setup in an anechoic chamber.

properly at the targeted frequency. The optimized spacing between the patches is set to 5.85 mm.

Fig. 12(a) shows the simulated and measured reflection coefficients of the patch array. The simulated (black) impedance bandwidth is observed to be in the range of 32.5–33.8 GHz while the measured (red) impedance bandwidth is observed to be in the range of 32.9–33.5 GHz, covering the targeted frequency of 33 GHz. The simulated (black) and measured (red) radiation patterns of the patch array at 33 GHz are shown in Fig. 12(b). It can be seen that the measured radiation pattern follows closely with the simulated one, with the maximum broadside gain being 18 dBi and 19.2 dBi, respectively.

B. DESIGN OF RECTIFIER TO CONVERT RF SIGNAL INTO DC POWER

In this subsection, the design of the rectifier is presented. The role of the rectifier is to convert RF power received by the patch array into DC power. As shown in Fig. 13, the rectifier is designed as a voltage doubler type, comprising two MA4E1317 Schottky diodes with a DC pass filter, DC block, matching network, and load resistor.

The rectifier design is carried out using Advanced Design System (ADS), first by verifying the DC pass filter. As a DC pass filter should suppress both fundamental and harmonics while efficiently transmit DC, four radial stubs are utilized. The radius of the first two stubs is originally set to a quarter-wavelength of the fundamental frequency (33 GHz) to suppress the fundamental while the radius of the other two stubs is originally set to quarter-wavelength of the second harmonic for harmonic suppression [34]. Each radius is then optimized by slightly adjusting it from the quarter-wavelength to maximize the suppression level. After verifying the performance of the DC pass filter via simulation, the impedance of the circuit, which includes the DC block, the diode, and the DC pass filter, is obtained in order to design a matching network. For the diode model, we utilized the equivalent circuit parameters of MA4E1317 provided in [35]. To match 50 Ω at the target frequency, an open parallel stub and series microstrip line is added. The lengths of the series microstrip line and the parallel open stub are calculated to be 0.66 λ (4.2 mm) and 0.4 λ(2.7 mm), respectively. Based on these calculated values, the overall circuit is optimized to minimize losses as much as possible. Consequently, the rectifier operates in the frequency range of 32.7 GHz to 33.35 GHz as depicted in Fig. 14(a).

The designed rectifier is then fabricated on the same substrate as that used for the patch array, and the rectification performance of the rectifier is conducted with an Agilent E8247C signal generator and voltmeter at the output of the rectifier. Fig. 14(b) compares the simulated and measured rectification efficiency with a load resistance of 300 Ω. The highest simulated efficiency is 37.8% at an input power of 23 dBm while the highest measured efficiency is 36.7% at an input power level of 23.6 dBm, indicating that the rectifier's peak efficiency has been well-realized. However, a discrepancy in efficiency can be observed up to the input power level of 20 dBm. The observed variation seems to have occurred due to the additional parasitic inductance and capacitance introduced when soldering the diode onto the PCB. This can be more prominent at mmWaves frequencies compared to microwave frequencies.

As can be seen in references such as [36], [37], [38], there has been recent development in improving the efficiency of mmWave rectifiers, some exhibiting an efficiency over 60%. However, since the aim of this paper is not primarily the design of the rectifier, but rather an experimental demonstration of the proposed end-to-end power beaming concept, we proceed with the current specifications of the rectifier, which can be further improved.

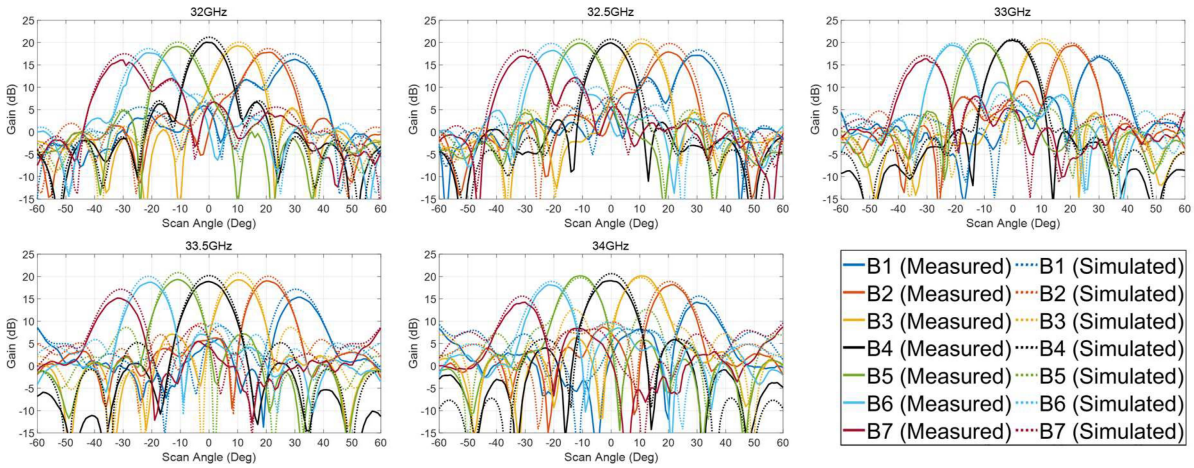

FIGURE 9. Radiation patterns of fabricated Rotman lens at frequencies ranging from 32 GHz to 34 GHz.

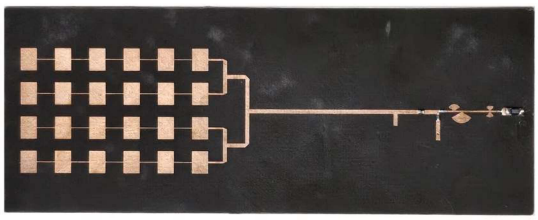

FIGURE 10. Fabricated structure of designed rectenna.

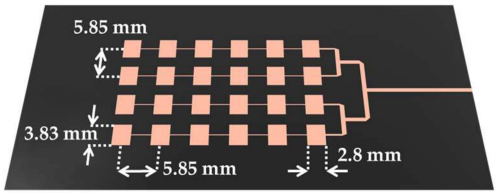

FIGURE 11. Design of the microstrip patch array as a part of the rectenna.

IV. END-TO-END POWER BEAMING TEST

Using the components discussed in the previous sections, an experimental apparatus for the end-to-end power beaming test is constructed. In order to demonstrate the scalability of this experimental system to a full system operation, the experiment is conducted in two separate stages. The first stage consists of sending a beacon signal from the location of the Rx unit, which will then be received by the Tx unit (Rotman lens). The direction from which the beacon signal came in is then determined for retrodirective transmission of wireless power. The second stage consists of the Tx unit transmitting power back to the location from where the beacon signal is sent, enabling retrodirective wireless power transfer.

The first stage of the experiment is illustrated in Fig. 15, which represents the process where the beacon signal is sent from the location of the Rx unit to the Tx unit. In a practical system, the Rx unit sending a beacon signal is typically integrated within the device itself. Here, we utilize a standard

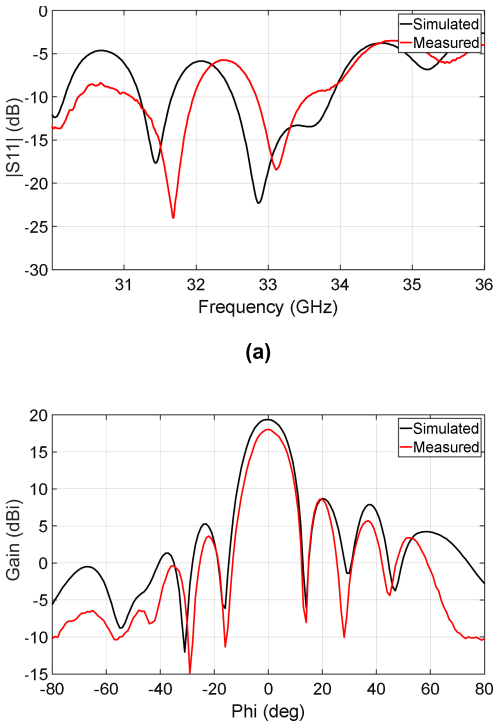

FIGURE 12. Simulated and measured (a) reflection coefficients, (b) radiation pattern of the patch antenna at 33 GHz.

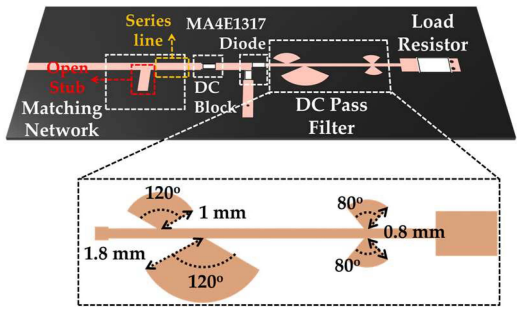

FIGURE 13. Geometric figure of the designed rectifier.

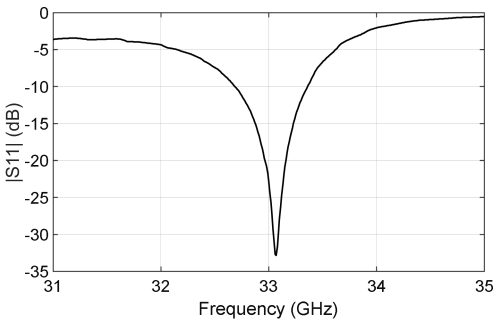

(a)

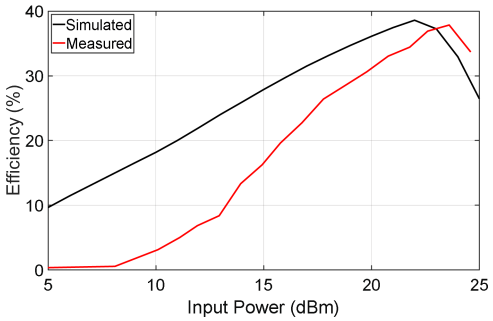

(b)

FIGURE 14. (a) Simulated reflection coefficient, (b) simulated and measured rectification efficiency at 33 GHz.

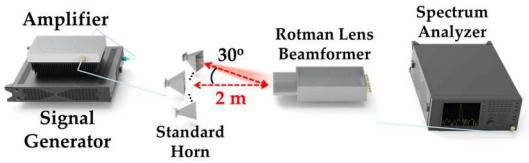

FIGURE 15. Test setup for transmitting beacon signal to the TX unit (Rotman lens).

gain horn as a separate transmitter for Rx unit. An Agilent E8247C signal generator and RFLUPA18G45G32CDK amplifier is used to generate the beacon signal at 33 GHz with the total power of 34 dBm (≈ 2.5 Watts). The Tx unit (Rotman lens) is located 2 m away from the horn. As shown in the Fig. 15, the horn's position is varied over −30° to 30° with an increment of 10°. At each position, the horn transmits the beacon signal, which is then received by the Tx unit (Rotman lens). Fig. 16 shows the measured received power with the Rotman lens through all the beam ports at each angle. It can be seen that the received power level peaks at the beam port that corresponds to the angle from which the beacon signal is sent, indicating that the beacon signal has successfully arrived at the appropriate beam port.

The second stage of the experiment is to transmit power retrodirectively back to the Rx unit. Note that in a notional system, a T/R module should be included, which will switch the Tx unit from the beacon receive mode to the power transmit mode, where amplified power signal will be transmitted

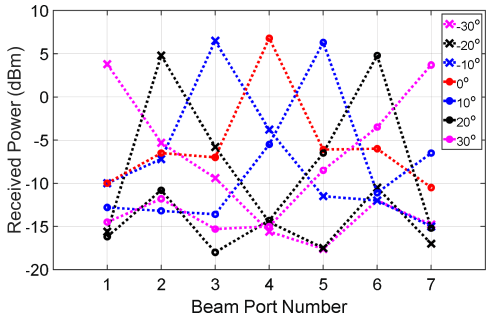

FIGURE 16. Measured power received by Rotman lens at each port at each radiation degree.

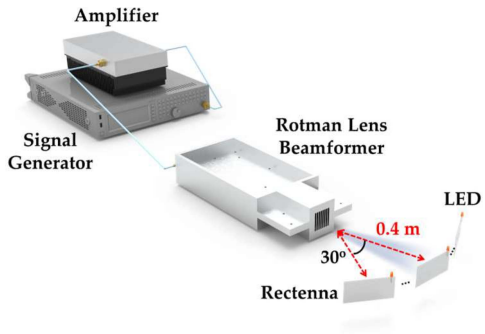

FIGURE 17. Lab environment of retrodirectively transmitting power to Rx unit (rectenna).

through the same beam port where the beacon signal came in. Here, the role of the T/R module is omitted for simplification of the experiment. The power beaming at the angles used in the first stage is demonstrated by directly feeding the respective beam ports from a power amplifier. The power beaming results are verified by placing multiple rectennas terminated with light emitting diodes (LEDs) at and off the intended angle, as illustrated in Fig. 17. The power source consists of the signal generator followed by the power amplifier, whose output is directly connected to the Rotman lens. With a little modification of the Friis equation, we can presume the power incident at the rectenna and set the distance to illuminate the LED that possess a turn-on voltage of 1.7 V as

$$V_{rec} = \sqrt{\frac{P_t \cdot G_{t\_Rotman} \cdot G_{r\_Patch} \cdot \lambda^2}{(4\pi R)^2} e_{rec} \cdot R_{load}}, \qquad (11)$$

where V_{rec} is the output DC voltage rectified by the rectenna, P_t is transmit power, G_{r_Patch} is the gain of the patch array, e_{rec} is the rectification efficiency of the rectifier, and R_{load} is the load resistance. Considering the maximum P_t (2.5 W) of the amplifier used in the experiment, the allowable distance for turning on the LED is determined to 0.4 m. The test is then performed by setting the distance between Tx and Rx at 0.4 m. The top photograph in Fig. 18 confirms that the output DC voltage measured with a voltmeter is 1.76 V, which is sufficient for turning the LED on. Also, the power beaming test is carried out at the seven angles used in the first stage (i.e., −30° − 30° with an increment of 10°). Around each

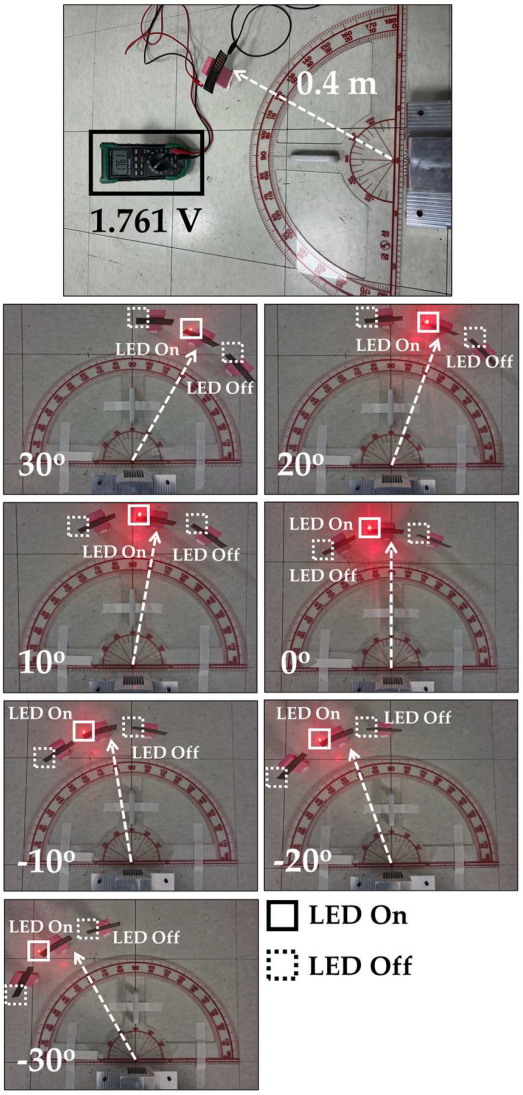

FIGURE 18. Output DC voltage measured with a voltmeter and power supplement to rectenna to turn the LED on.

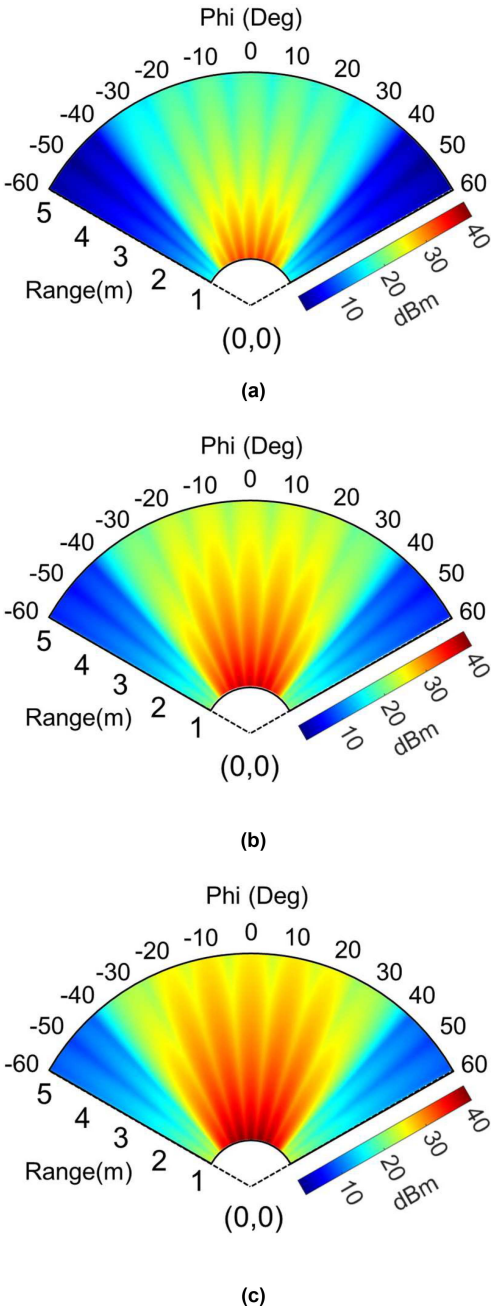

FIGURE 19. Calculated received power when transmit power is (a) 50 Watts, (b) 150 Watts, and (c) 250 Watts.

intended angle, three sets of LED-terminated rectennas are positioned: one at the intended angle and the other two at off the angle (±20° at the intended angle). In Fig. 18, it is observed that only the LED positioned at the intended angle is turned on while the other LEDs remain unlit, indicating that the Rotman lens beamformer has successfully transmitted the power retrodirectively to the direction of the Rx unit.

V. DISCUSSION

While the experiment described above demonstrates the proposed concept, limited Tx output power only allowed the experiment to be carried out at a closer range. Here, we discuss the scalability and expandability of the proposed power beaming system to a further range. Fig. 19 plots the power received when transmitting with the proposed Tx unit (Rotman lens) and receiving with the same Rx unit as used above. Assuming that the beamformer is located at the origin (0,0) and retrodirectively scans the area with a transmit power of 50 Watts, it can be seen that the maximum power received through the Rx unit is approximately 33 dBm at 1 m and less than 25 dBm at 5 m in the beam scan range (Fig. 19(a)). When the beamformer transmits 150 Watts of power, at least 27 dBm of power is received (Fig. 19(b)). Also, the received power ranges from 30 dBm to 40 dBm when the transmit power is 250 Watts (Fig. 19(c)). If higher power is transmitted with the beamformer with higher gain, and the RF-to-DC rectification efficiency of the rectenna is improved, it can potentially scale up to a level high enough to charge the devices requiring

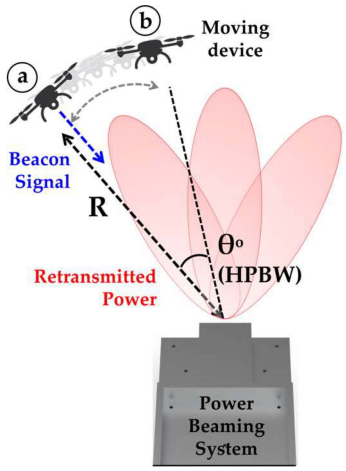

FIGURE 20. Conceptual illustration of the power beaming system in a dynamic environment.

higher power. Therefore, how the system can be configured will depend on the devices to be powered, minimum power beaming distance, available source, etc.

As mentioned in the introduction, the essence of utilizing retrodirectivity is that it can precisely direct the power at the receiver upon the receipt of a beacon signal sent from the device. This can be effectively applied to stationary objects. However, whether the retrodirective operation is feasible even in a dynamic environment (e.g., flying drones, a device held by a moving person, etc.) is an important consideration.

For retrodirective operation to be effectively applied in a dynamic environment, a certain condition should be satisfied. The process of the power beaming system receiving a beacon signal and retrodirectively transmitting power back to the device should be fast enough to track the device's movement. That is the device needs to be maintained within the half-power beamwidth (HPBW) of the beam. Therefore, the system's full retrodirective operation time should be shorter than the time it takes for the device to move outside the HPBW. Fig. 20 illustrates a simple scenario of a dynamic environment where the power beaming system tracks a moving device. To simplify the calculation, few assumptions are made. The device has a velocity of v(m/s) and the system has a HPBW of θ^o. When the device sends a beacon signal from point 'a' which is R m away from the system and moves toward point 'b', the system should be able to retransmit power back at the device before it passes point 'b'. Therefore, the maximum time, t, required for the system to track the device is determined as

$$t = \frac{2\pi R \frac{\theta}{360}}{v} \text{ [s]}. \tag{12}$$

If the process of receiving beacon signals and analyzing them to determine the retrodirective transmit port can be achieved within t, the proposed retrodirective approach can also be applied to dynamic environment.

VI. CONCLUSION

In this paper, a mmWave retrodirective power beaming system was proposed and tested with an experimental apparatus. In particular, the design of two main critical components for the Tx and Rx units, namely a Rotman lens beamformer and rectenna, respectively, were presented. Via simulation and measurements, the performance of both the Rotman lens beamformer and rectenna were verified. Furthermore, the power beaming experiment was conducted with the proposed components, where the results demonstrated the capability of the proposed system as a retrodirective mmWave power beaming system. The scalability of the proposed concept to higher power and longer range was also highlighted, indicating the proposed system's potential in wireless power beaming of small electronic devices.

REFERENCES

[1] O. B. Akan, O. Cetinkaya, C. Koca, and M. Ozger, "Internet of hybrid energy harvesting things," *IEEE Internet Things J.*, vol. 5, no. 2, pp. 736–746, Apr. 2018.
[2] M. A. Hoque, M. Hossain, S. Noor, S. M. R. Islam, and R. Hasan, "IoTaaS: Drone-based internet of Things as a service framework for smart cities," *IEEE Internet Things J.*, vol. 9, no. 14, pp. 12425–12439, Jul. 2022.
[3] W. C. Brown, "The history of power transmission by radio waves," *IEEE Trans. Microw. Theory Techn.*, vol. TMTT-32, no. 9, pp. 1230–1242, Sep. 1984.
[4] W. Na, J. Park, C. Lee, K. Park, J. Kim, and S. Cho, "Energy-efficient mobile charging for wireless power transfer in Internet of Things networks," *IEEE Internet Things J.*, vol. 5, no. 1, pp. 79–92, Feb. 2018.
[5] K. W. Choi, A. A. Aziz, D. Setiawan, N. M. Tran, L. Ginting, and D. I. Kim, "Distributed wireless power transfer system for Internet of Things devices," *IEEE Internet Things J.*, vol. 5, no. 4, pp. 2657–2671, Aug. 2018.
[6] P. Wu, F. Xiao, H. Huang, C. Sha, and S. Yu, "Adaptive and extensible energy supply mechanism for UAVs-aided wireless-powered Internet of Things," *IEEE Internet Things J.*, vol. 7, no. 9, pp. 9201–9213, Sep. 2020.
[7] M. Tavana, M. Ozger, A. Baltaci, B. Schleicher, D. Schupke, and C. Cavdar, "Wireless power transfer for aircraft IoT applications: System design and measurements," *IEEE Internet Things J.*, vol. 8, no. 15, pp. 11834–11846, Aug. 2021.
[8] C. T. Rodenbeck et al., "Microwave and millimeter wave power beaming," *IEEE J. Microwaves*, vol. 1, no. 1, pp. 229–259, Jan. 2021.
[9] R. M. Dickinson and W. C. Brown, "Radiated microwave power transmission system efficiency measurements," NASA Tech., Pasadena, CA, USA, Tech. Rep. JPL-TM-33-727, May 1975.
[10] V. R. Gowda, O. Yurduseven, G. Lipworth, T. Zupan, M. S. Reynolds, and D. R. Smith, "Wireless power transfer in the radiative near field," *IEEE Antennas Wireless Propag. Lett.*, vol. 15, pp. 1865–1868, 2016.
[11] K. Dang et al., "A 5.8-GHz high-power and high-efficiency rectifier circuit with lateral GaN Schottky diode for wireless power transfer," *IEEE Trans. Power Electron.*, vol. 35, no. 3, pp. 2247–2252, Mar. 2020.
[12] Q. Hui, K. Jin, and X. Zhu, "Directional radiation technique for maximum receiving power in microwave power transmission system," *IEEE Trans. Ind. Electron.*, vol. 67, no. 8, pp. 6376–6386, Aug. 2020.
[13] J. Charthad, N. Dolatsha, A. Rekhi, and A. Arbabian, "System-level analysis of far-field radio frequency power delivery for mm-sized sensor nodes," *IEEE Trans. Circuits Syst. I, Reg. Papers*, vol. 63, no. 2, pp. 300–311, Feb. 2016.
[14] T. A. Khan, A. Alkhateeb, and R. W. Heath, "Millimeter wave energy harvesting," *IEEE Trans. Wireless Commun.*, vol. 15, no. 9, pp. 6048–6062, Sep. 2016.
[15] M. Molefi, E. D. Markus, and A. Abu-Mahfouz, "Wireless power transfer for IoT devices – a review," in *Proc. Int. Multidisciplinary Inf. Technol. Eng. Conf.*, Vanderbijlpark, South Africa, 2019, pp. 1–8.

[16] Z. Cai, Y. Zhou, Y. Qi, W. Zhuang, and L. Deng, "A millimeter wave dual-lens antenna for IoT-based smart parking radar system," *IEEE Internet Things J.*, vol. 8, no. 1, pp. 418–427, Jan. 2021.
[17] M. Wagih, G. S. Hilton, A. S. Weddell, and S. Beeby, "Millimeter-wave power transmission for compact and large-area wearable IoT devices based on a higher order mode wearable antenna," *IEEE Internet Things J.*, vol. 9, no. 7, pp. 5229–5239, Apr. 2022.
[18] J. G. D. Hester and M. M. Tentzeris, "Inkjet-printed flexible mm-wave Van-Atta reflect arrays: A solution for ultralong-range dense multitag and multisensing chipless RFID implementations for IoT smart skins," *IEEE Trans. Microw. Theory Techn.*, vol. 64, no. 12, pp. 4763–4773, Dec. 2016.
[19] S. -T. Khang, D. -J. Lee, I. -J. Hwang, T. -D. Yeo, and J. -W. Yu, "Microwave power transfer with optimal number of rectenna arrays for midrange applications," *IEEE Antennas Wireless Propag. Lett.*, vol. 17, no. 1, pp. 155–159, Jan. 2018.
[20] T. Sasaki and N. Shinohara, "Study on multipath retrodirective for efficient and safe indoor microwave power transmission," in *Proc. IEEE Wireless Power Transfer Conf.*, London, U.K., 2019, pp. 329–333.
[21] H. Y. Hong et al., "Ka-band Rotman lens-based retrodirective beamforming system for wireless power transfer," *J. Electromagn. Eng. Sci.*, vol. 21, no. 5, pp. 391–398, Nov. 2021.
[22] X.-F. Li, Y.-L. Ban, Q. Sun, Y.-X. Che, and J. Hu, "Compact dual-frequency 2-D van Atta array using the reconfigurable AMC antenna," *IEEE Antennas Wireless Propag. Lett.*, vol. 22, no. 12, pp. 3162–3166, Dec. 2023.
[23] W. Rotman and R. Turner, "Wide-angle microwave lens for line source applications," *IEEE Trans. Antennas Propag.*, vol. TAP-11, no. 6, pp. 623–632, Nov. 1963.
[24] R. C. Hansen, "Design trades for Rotman lenses," *IEEE Trans. Antennas Propag.*, vol. 39, no. 4, pp. 464–472, Apr. 1991.
[25] P. S. Simon, "Analysis and synthesis of Rotman lenses," in *Proc. 22nd AIAA Int. Commun. Satell. Syst. Conf. Exhibit*, Monterey, CA, USA, 2004, p. 3196.
[26] E. H. Mujammami, I. Afifi, and A. B. Sebak, "Optimum wideband high gain analog beamforming network for 5G applications," *IEEE Access*, vol. 7, pp. 52226–52237, 2019.
[27] A. Eid, J. G. D. Hester, and M. M. Tentzeris, "Rotman lens-based wide angular coverage and high-gain semipassive architecture for ultralong range mm-wave RFIDs," *IEEE Antennas Wireless Propag. Lett.*, vol. 19, no. 11, pp. 1943–1947, Nov. 2020.
[28] W. Lee, J. Kim, and Y. J. Yoon, "Compact two-layer Rotman lens-fed microstrip antenna array at 24 GHz," *IEEE Trans. Antennas Propag.*, vol. 59, no. 2, pp. 460–466, Feb. 2011.
[29] A. Attaran, R. Rashidzadeh, and A. Kouki, "60 GHz low phase error Rotman lens combined with wideband microstrip antenna array using LTCC technology," *IEEE Trans. Antennas Propag.*, vol. 64, no. 12, pp. 5172–5180, Dec. 2016.
[30] K. Tekkouk, M. Ettorre, L. Le Coq, and R. Sauleau, "Multibeam SIW slotted waveguide antenna system fed by a compact dual-layer Rotman lens," *IEEE Trans. Antennas Propag.*, vol. 64, no. 2, pp. 504–514, Feb. 2016.
[31] K. Tekkouk, M. Ettorre, and R. Sauleau, "SIW Rotman lens antenna with ridged delay lines and reduced footprint," *IEEE Trans. Microw. Theory Techn.*, vol. 66, no. 6, pp. 3136–3144, Jun. 2018.
[32] Y. F. Wu, Y. J. Cheng, and Z. X. Huang, "Ka-band near-field-focused 2-D steering antenna array with a focused Rotman lens," *IEEE Trans. Antennas Propag.*, vol. 66, no. 10, pp. 5204–5213, Oct. 2018.
[33] W. L. Stutzman and G. A. Thiele, *Antenna Theory and Design*, 3rd ed. Hoboken, NJ, USA: Wiley, 2012.
[34] S. Ladan and K. Wu, "Nonlinear modeling and harmonic recycling of millimeter-wave rectifier circuit," *IEEE Trans. Microw. Theory Techn.*, vol. 63, no. 3, pp. 937–944, Mar. 2015.
[35] S.-P. Gao, W. Hu, H. Zhang, and Y. Guo, "Millimeter-wave rectifiers using proprietary Schottky diodes: Diode modeling and rectifier analysis," in *Proc. Wireless Power Week*, Bordeaux, France, Jul. 2022, pp. 180–184.
[36] Q. Chen, X. Chen, H. Cai, and F. Chen, "A waveguide-fed 35-GHz rectifier with high conversion efficiency," *IEEE Microw. Wireless Compon. Lett.*, vol. 30, no. 3, pp. 296–299, Mar. 2020.
[37] Y. Wang, X.-X. Yang, G.-N. Tan, and S. Gao, "Study on millimeter-wave SIW rectenna and arrays with high conversion efficiency," *IEEE Trans. Antennas Propag.*, vol. 69, no. 9, pp. 5503–5511, Sep. 2021.
[38] C. Song et al., "Highly efficient wideband mmWave rectennas for wireless power transfer system with low-cost multinode tracking capability," *IEEE Trans. Antennas Propag.*, vol. 71, no. 11, pp. 8773–8787, Nov. 2023.

SOOYOUNG OH (Graduate Student Member, IEEE) received the B.S. degree in electronic engineering in 2021 from Soongsil University, Seoul, South Korea, where he is currently working toward the Ph. D. degree in electronic engineering. His research interests include nonlinear radar, radar signal processing, mmWaves wireless power transfer, and quantum computing.

DO HYEON KIM (Graduate Student Member, IEEE) received the B.S. degree in electronic engineering from Sunmoon University, Asan, South Korea, in 2018. He is currently working toward the Ph. D. degrees with Soongsil University, Seoul, South Korea. His research interests include wireless power transfer, mmWave devices, high-power electromagnetics, and quantum computing.

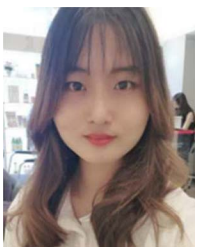

WONWOO LEE received the B.S. and M.S. degrees in electronic engineering and the Ph.D. degree in information communication convergence technology from Soongsil University, Seoul, South Korea, in 2016, 2018, and 2023, respectively. She is currently a Postdoctoral Researcher with Soongsil University. Her research interests include microwave energy-harvesting metamaterial based chemical sensor, mmWave electromagnetic focusing metasurface lens, and terahertz metamaterial design, fabrication, and analysis.

JUNHYUK YANG received the B.S. and M.S. degrees in electronic engineering from Soongsil University, Seoul, South Korea, in 2019 and 2021, respectively. His research interests include wireless power transfer and mmWave integrated circuits.

CHANGKUN PARK (Member, IEEE) received the B.S., M.S., and Ph.D. degrees in electrical engineering from the Korea Advanced Institute of Science and Technology, Daejeon, South Korea, in 2001, 2003, and 2007, respectively. From 2007 to 2009, he was with the Advanced Design Team of the DRAM Development Division, Hynix Semiconductor Inc., Icheon, South Korea, where he was involved in development of high-speed I/O interfaces of DRAM. In 2009, he joined the faculty of the School of Electronic Engineering, Soongsil University, Seoul, South Korea. His research interests include RF and millimeter-wave circuits, wireless chip-to-chip communications, and power transfers.

HOJIN LEE (Member, IEEE) received the B.S. and M.S. degrees in electrical engineering from Hanyang University, Seoul, South Korea, in 1996 and 1998, respectively, and Ph.D. degree in electrical engineering and computer science from the University of Michigan, Ann Arbor, MI, USA, in 2008. He is currently an Assistant Professor with the School of Electronic Engineering, Soongsil University, Seoul. He has authored or coauthored more than 40 research papers in refereed journals and a number of conference papers presented at international conferences. His research interests include display circuit design, OLED fabrication development, chemical sensor device development, ionic polymer-based actuator, mmWave and terahertz metamaterial, and wireless power transfer system for bio-implantable device.

SUN K. HONG (Senior Member, IEEE) received the B.S. degree in electrical engineering from the University of Maryland, College Park, MD, USA, in 2005, and the M.S. and Ph.D. degrees in electrical engineering from Virginia Tech, Blacksburg, VA, USA, in 2008 and 2012, respectively. He is currently an Associate Professor with the School of Electronic Engineering, Soongsil University, Seoul, South Korea. From 2005 to 2015, he was a Research Engineer with the U.S. Naval Research Laboratory, Washington, DC, USA, where he was involved in research related to time-domain techniques in electromagnetics, nonlinear electromagnetic interaction, radars, electromagnetic scattering, high power microwave (HPM) applications, and antennas. From 2015 to 2017, he was an Assistant Professor with the Department of Electrical and Computer Engineering, Rose-Hulman Institute of Technology, Terre Haute, IN, USA. Since 2017, he has been with Soongsil University. His research interests include wavefront control techniques, wireless power transfer, EM waves in complex propagation environment, detection of nonlinear devices, radars, and high-power electromagnetics and antennas.